Synchrotron-based high angle resolution and high lateral resolution X-ray diffraction reveals lead white pigment qualities in Old Masters paintings

Victor Gonzalez, Gilles Wallez, Thomas Calligaro, Marine Cotte, Wout de Nolf, Myriam Eveno, Elisabeth Ravaud, Michel Menu

Article

Synchrotron-based high angle resolution and high lateral resolution X-ray diffraction reveals lead white pigment qualities in Old Masters paintings

Victor Gonzalez, Gilles Wallez, Thomas Calligaro, Marine Cotte, Wout De Nolf, Myriam Eveno, Elisabeth Ravaud, and Michel Menu

Anal. Chem., **Just Accepted Manuscript** • DOI: 10.1021/acs.analchem.7b02949 • Publication Date (Web): 14 Nov 2017

Synchrotron-based high angle resolution and high lateral resolution X-ray diffraction reveals lead white pigment qualities in Old Masters paintings

V. Gonzalez*[1,2,3], G. Wallez[2,3,1], T. Calligaro[1,2], M. Cotte[4,5], W. De Nolf[4], M. Eveno[1], E. Ravaud[1] and M. Menu[1,2]

[1]Centre de Recherche et de Restauration des Musées de France, C2RMF, Palais du Louvre, 75001 Paris, France
[2]PSL Research University, Chimie ParisTech - CNRS, Institut de Recherche de Chimie Paris, UMR8247, 75005 Paris, France
[3]Sorbonne University, UPMC Univ. Paris 06, France
[4]European Synchrotron Radiation Facility, BP-220, Grenoble Cedex, 38043, France
[5]Laboratoire d'Archéologie Moléculaire et Structurale (LAMS), Sorbonne University, UPMC Univ. Paris 06, France

ABSTRACT: Micro-samples collected on 27 major paintings by Old European Masters dating from the 14th to the late 19th c. were analyzed using Synchrotron-based X-ray diffraction. Two complementary analytical configurations were used at beamlines ID22 (high-angle resolution) and ID21 (high lateral resolution), in order to highlight markers of the different grades of the lead white pigments (mixture of cerussite $PbCO_3$ and hydrocerussite $Pb_3(CO_3)_2(OH)_2$). Rietveld analysis and crystalline phases mapping at the micro-scale revealed the composition and microstructure of the pigments, shedding light on the preparation recipes and pigment choices of the artists through History.

Until the 20th c., lead white has been one of the most employed pigments in easel paintings[1]. Lead white is commonly composed of two crystalline phases, cerussite $PbCO_3$ (*C*) and hydrocerussite $Pb_3(CO_3)_2(OH)_2$ (*HC*). Cerussite has an orthorhombic (space group *Pmcn*) aragonite-type structure (a = 5.179 Å, b = 8.492 Å, c = 6.141 Å)[2]. Hydrocerussite belongs to the rhombohedral system (space group *R*-3*m*), with lattice parameters a = 5.246 Å, c = 23.702 Å[3]. In aqueous conditions, the formation of the two phases is *p*H dependent: C in acidic (*p*H < 6) and HC in basic (8 < *p*H < 10) environment. Morphologies (size and shapes) of the two phase crystallites can significantly vary, but most generally, cerussite crystallites are elongated along the [100] direction[4], and hydrocerussite tends to crystallize as hexagonal platelets[5, 6].

The synthesis of lead white has remained almost unchanged from the Antiquity until the 19th c.[7]. It was traditionally based on the corrosion of metallic lead. Rows of jars containing lead plaques suspended above vinegar were stacked under horse manure: the decomposition of the manure produced CO_2 and heat[8]. The combination of those reactants with acetic acid vapors induced the formation of cerussite and hydrocerussite at the surface of the lead[9]. The pigment was collected before being sold to painters.

Historical sources reveal that some synthesis parameters could be adjusted, such as the time of corrosion. In addition, the obtained raw material was almost systematically post-processed by paint manufacturers or painters themselves before being mixed with the organic binder and employed in a painting[10]. Numerous post-synthesis treatments were used in color shops and artist's workshops[11], such as washing and grinding the pigment in various media (vinegar, water), or heating in water. Obviously, these different processing and post-processing steps impact the chemical and physical characteristic of the final pigment. According to the sophistication degree of the *chaine opératoire* applied to the pigment, different grades were obtained and proposed at very different prices on color markets[12, 13].

Scope

The present work aims at detecting potential markers that could reveal the various pigment qualities used in European artworks, painted between the Middle Ages and the 19th c. and relate them to production recipes. Indeed, the variation of synthesis conditions and the

application of post-synthesis treatments induce changes in the composition (in particular *HC*:*C* ratio) and the microstructure of lead white (crystallites morphology)[14]. Those two parameters are accessible in historic paint micro-samples collected on artworks, using Synchrotron radiation (SR)-based X-ray diffraction (XRD).

In this work we report results obtained by SR-high-angular resolution-XRD (SR-HXRD) and SR-high lateral resolution-XRD (SR-μXRD) on a corpus of 36 samples. SR-HXRD is essential to obtain high quality XRD data (and consequently quantitative phase composition and crystallite morphologies), however it requires large and homogeneous samples. As a complement, μXRD was used for the qualitative analysis of complex multi-layered samples. The studied fragments were sampled from major artworks, preserved in French museums and covering a long historical period, ranging from the Middle Ages to the 19th c. (the oldest sample was collected on the Louvre's *Cross* by Giotto (1267-1337), while the most recent came from the *Self-Portrait* by van Gogh (1853-1890) conserved in the Orsay Museum). The complete list is presented in Table 1. Within this corpus, two artworks from the Louvre Museum samples were of particular interest, as the materials used during their conception have been documented in historical sources. More specifically, the question concerns the use of a particular quality of pigment in artworks commissioned by the Burgundy court during the 14th c. The accounts of the court that have been recently investigated report the purchase of two white pigment types, at different prices: the « *blanc de plomb* [= lead white] » and the « *blanc de puille* [= puille white] »[15]. The precise nature of *blanc de puille* is unknown to art historians: the only certitude is that it was bought at a lower price (twice as low) than *blanc de plomb*. The first sample has been collected on the *Calvaire avec un moine chartreux* (c. 1395) (Fig. 1A) by Jean de Beaumetz (1335-1396), the second on the *Retable de Saint-Denis* (1416) (Fig. 1B), by Henri Bellechose (fl. 1415-1444). Historical sources indicate that while Bellechose used *blanc de plomb*, Beaumetz chose *blanc de puille*.

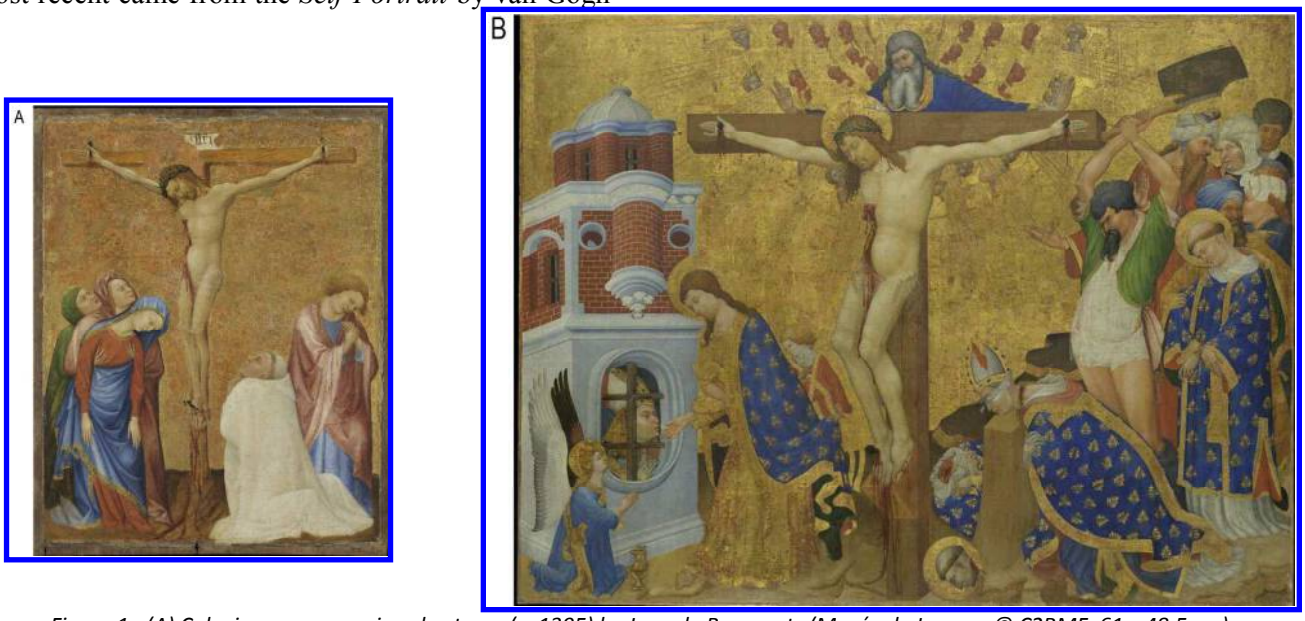

Figure 1 : (A) Calvaire avec un moine chartreux (c. 1395) by Jean de Beaumetz (Musée du Louvre, © C2RMF, 61 x 48.5 cm). (B) Retable de Saint Denis (1416) by Henri Bellechose (Musée du Louvre, © C2RMF, 162 x 211 cm)

MATERIALS AND METHODS

Samples

Historical samples selected for this work belong to the C2RMF samples collection and are paint micro-fragments previously collected on masterpieces conserved in several French Museums, particularly the Louvre and Orsay (Paris, France).

Micro samples have dimensions typically inferior to 100 μm. They were available under two forms: as raw fragments (32 samples) and as cross-sections prepared by polishing samples embedded in resin (two samples).

For HR-XRD experiments, raw samples were placed in sealed glass capillaries and positioned directly in

front of the X-ray beam of the ID22 beamline. A limit of the HR-XRD analytical configuration lies in the lateral resolution. With a beam of 1 mm², the whole bulk of the sample is analyzed simultaneously: in the case of complex stratifications, contributions of all the layers are mixed in the obtained diffractogram. In our case, we selected samples with only one layer containing lead white. In one particular case, it was possible to carefully mechanically separate two superimposed lead white-based layers, in order to analyzed them separately (see Table 1, samples 3-a and 3-b), but this process is very tedious and cannot be routinely performed.

Table 1 : Historical micro-samples analyzed by HR-XRD and µXRD

Painter	Artwork	Nature of sample	Analytical method	Label used in figures
Giotto (1266/76-1337)	*Crucifix* (c. 1315)	Layer	HR-XRD	Giotto
Master of 1333 (active c. 1325-1350)	*Retable* (1333)	Layer	HR-XRD	Maitre1333
Jean de Beaumetz (1335-1396)	*Calvaire avec un moine chartreux* (c. 1395)	Complete stratigraphy	µXRD	Beaumetz
Henri Bellechose (active c. 1415-1444)	*Retable de Saint Denis* (1416)	Complete stratigraphy	µXRD	Bellechose
Giovanni da Camerino Boccati (1420-1480)	*Vierge à l'enfant et concert d'anges* (1463-1480)	Layer	HR-XRD	Boccati
Mantegna (c.1431-1506)	*Saint Sébastien* (1480)	Layer	HR-XRD	Mantegna
Botticelli (1444/45-1510)	*La Vierge et l'enfant avec un ange* (c. 1490)	Layer	HR-XRD	Botticelli 1
Botticelli (1444/45-1510)	*La Vierge et l'Enfant soutenu par un ange* (c. 1467-1510)	Layer	HR-XRD	Botticelli 2
Botticelli (1444/45-1510)	*La Vierge à l'enfant* (1444/45-1510)	Layer	HR-XRD	Botticelli 3
Leonardo da Vinci (1452-1519)	*La Belle Ferronnière* (1495-1497)	Ground	HR-XRD	Leonardo 1
Leonardo da Vinci (1452-1519)	*La Joconde* (1503/06)	Ground	HR-XRD	Leonardo 2
Leonardo da Vinci (1452-1519)	*La Vierge, l'enfant Jésus et sainte Anne* (c. 1508/10)	Layer	HR-XRD	Leonardo 3-a
Leonardo da Vinci (1452-1519)	*La Vierge, l'enfant Jésus et sainte Anne* (c. 1508/10)	Layer	HR-XRD	Leonardo 3-b
Leonardo da Vinci (1452-1519)	*La Vierge, l'enfant Jésus et sainte Anne* (c. 1508/10)	Priming	HR-XRD	Leonardo 3-c
Grünwald (1475/80-1528)	*Retable d'Issenheim* (c.1512-1516)	Layer	HR-XRD	Grünwald
Lotto (1480-1557)	*Le portement de croix* (1526)	Layer	HR-XRD	Lotto 1-a
Lotto (1480-1557)	*Le portement de croix* (1526)	Layer	HR-XRD	Lotto 1-b
Raffaello (1483-1520)	*La Belle Jardinière* (c. 1507-1508)	Layer	HR-XRD	Raffaello 1
Raffaello (1483-1520)	*Portrait de l'artiste avec un ami* (c. 1519)	Layer	HR-XRD	Raffaello 2
Raffaello (1483-1520)	*La Grande Sainte Famille* (1518)	Layer	HR-XRD	Raffaello 3
Bronzino (1503-1572)	*Sainte Famille* (c. 1550)	Layer	HR-XRD	Bronzino
Parmigianino (1503-1540)	*Portrait de jeune homme* (c.1520-1530)	Layer	HR-XRD	Parmigianino 1-a
Parmigianino (1503-1540)	*Portrait de jeune homme* (c.1520-1530)	Priming	HR-XRD	Parmigianino 1-b
Tintoretto (1518-1594)	*Le Paradis* (1579/80)	Layer	HR-XRD	Tintoretto
Contemporary of Goya	*Dernière communion de San José de Calasanz* (1819)	Ground	HR-XRD	Goya 1-a
Contemporary of Goya	*Dernière communion de San José de Calasanz* (1819)	Layer	HR-XRD	Goya 1-b
Goya (1746-1828)	*Portrait de la Solana* (1794-1795)	Layer	HR-XRD	Goya 2
Goya (1746-1828)	*Grande Marquise de Santa Cruz* (1798-1799)	Layer	HR-XRD	Goya 3
Monet (1840-1926)	*La cathédrale de Rouen. Le portail et la tour Saint-Romain, plein soleil. Harmonie bleu et or* (1893)	Ground	HR-XRD	Monet 1a
Monet (1840-1926)	*La cathédrale de Rouen* (1893)	Ground	HR-XRD	Monet 1b
Monet (1840-1926)	*La cathédrale de Rouen* (1893)	Transfer layer	HR-XRD	Monet 1c
Monet (1840-1926)	*La cathédrale de Rouen. Le portail, soleil matinal. Harmonie bleue* (1893)	Ground	HR-XRD	Monet 2
van Gogh (1853-1890)	*Le jardin à Auvers* (1853-1890)	Ground	HR-XRD	van Gogh 1
van Gogh (1853-1890)	*Portrait de l'artiste* (1889)	Ground	HR-XRD	van Gogh 2

In order to gain insight on more complex samples, it is necessary to work at a very good spatial resolution (micrometric scale), which was achieved at the ID21 X-ray microscopy beamline: spatial repartition of the crystalline phases can then be retrieved, providing an insight on the entire paint layers' stratification. Accordingly, µXRD was applied to a more reduced corpus, those presenting a complex multilayer structure.

For µXRD experiments, samples were prepared as thin sections (to allow measurements in transmission mode at 8.5 keV). These sections were obtained from historical samples in resin blocks, using a microtome. Their preparation was made difficult by the fact that some of the resin blocks had been prepared decades ago: the resin was not necessarily suitable for microtomy and it was important to preserve as much as the sample cross-section for future analyses. Accordingly, a dedicated protocol was optimized consisting in slicing the cross-section along one of its

sides, perpendicular to the cross-section surface, and perpendicular to the sample strates[16, 17]. In order to preserve the stratification in the thin section, a small piece of sulfur-free tape (Fluxana) is applied on the resin surface, trapping the thin section during the cut. This section can then be protected with an Ultralen foil (Spex Certiprep) avoiding the sample fragment to fall away. The complete protocol is detailed in S. I.

Analytical methods

XRD measurements were performed at two beamlines of the European Synchrotron Radiation Facility (ESRF, Grenoble, France).

SR-high-angular resolution-XRD. HR-XRD was carried out at ID22 beamline[18] (ESRF), which is equipped with a 9-channel Si (111) multianalyzer stage. Glass capillaries containing the raw paint micro-samples were placed in front of the 1×1 mm² beam. The capillaries were rotated at 12 rps during the experiment, to avoid preferential orientation effects. High energy radiation was selected (35 keV, 0.3542 Å) to ensure a good transparency (at this energy, the transmission factor for a micro-sample of 1-3 µg in weight composed of ~50 vol. % lead white is estimated around 60 %). Because of the small size of the samples, 20 min scans were repeated up to a total acquisition time of 1-4 h to record diffractograms with a good signal to noise ratio. The exploitable angular range was $2 \leq 2\theta$ (°) ≤ 22 ($0.93 \leq d$ (Å) ≤ 10.14), allowing the measurement of 152 reflections for *C* and 49 for *HC*. The main advantages of this configuration are the excellent angular resolution (0.002°) and the absence of preferential orientation. This permits the recording of high quality datasets: a precise composition can be derived from the Rietveld fitting[19] (error bars of about ±1 w% estimated from a *C*/*HC* calibration mixture) and the modeling of the pigment crystallite morphologies is possible. To achieve that, XRD patterns were analyzed using the Fullprof suite[20], on the basis of crystallographic data found in the literature for *HC*[3] and *C*[2] (Fig. 2A). Quantitative phase analyses were derived from the scale factors. More particularly, the *HC*/(*HC*+*C*) and $CaCO_3$/(*HC*+*C*) weight percentages were calculated to assess the pigment composition. More details on the Rietveld fitting can be found elsewhere[14].

For the assessment of crystallites sizes, a measurement was considered as reliable only in the case of a sufficient broadening (> 50%), that is for crystallites of size < 1.5 µm (for a full-width at half maximum FWHM of the instrumental peak (LaB_6) of 0.004° at 2θ = 10°). In other words, the modeling is only possible for small crystallites. More particularly, for *HC*, the overview of the mean crystallites sizes is solely based on the thickness of the hexagonal platelets (l_c).

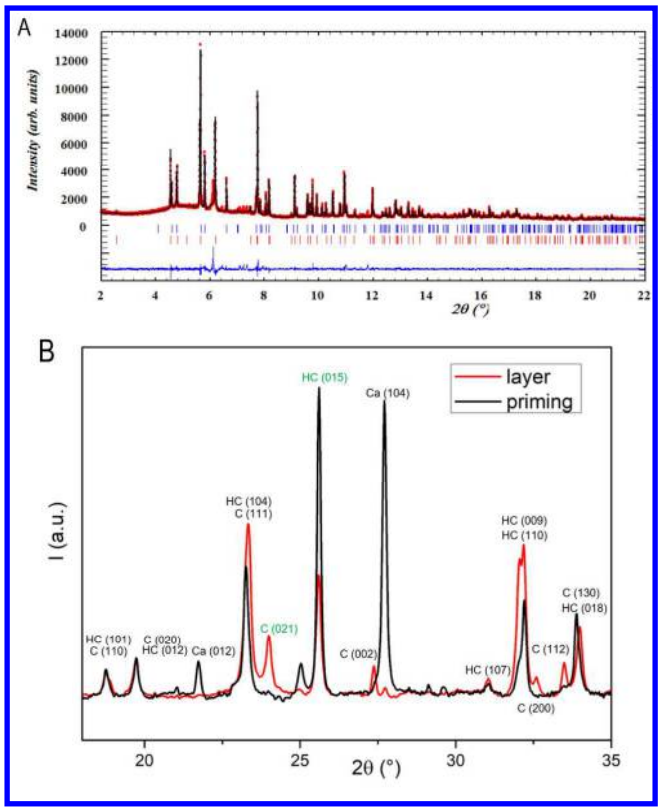

Figure 2 : (A) Rietveld plot for diffractogram recorded by HR-XRD at ID22 (sample Rafaello 1) : experimental (red circles), calculated (black line), difference (blue line), Bragg positions (bars). (B) Cumulated and azimuthally integrated diffractogram recorded by µXRD at ID21 on layer 3 of sample Beaumetz (cf. Fig 7). Peaks used for quantification ($C_{(021)}$ and $HC_{(015)}$) are indicated in green.

SR-high lateral resolution-XRD. µXRD experiments were carried out at the ID21 beamline, ESRF. This beamline offers a combination of multiple micro-analytical X-ray based techniques[21]. For this work, the µXRD branch was used to perform crystalline phase mapping using a 0.7×1.0 µm² beam. In this mode, the beamline is optimized for an energy of 8.54 keV, 1.4519 Å. 2D diffraction patterns (Debye-Scherrer rings) are recorded in transmission, on a CCD FReLON camera (2048×2048 pixels, 52 µm

pixel size) positioned behind the sample. The diffraction rings are then converted into 1D diffractograms by azimuthal integration, using the PyFAI and XRDUA softwares[22, 23]. Thin-sections are positioned on a motorized *xyz* stage, perpendicular to the beam, and are then raster scanned over a 2D map. At each pixel, a diffractogram is recorded: crystalline phases distribution for the entire mapped area is thus performed. The XRDUA software package was used to handle μXRD data[24]. In particular, the diffractogram recorded at each pixel of the map was fitted on the basis of references for each crystalline phase of interest. Background correction was also applied. This allowed obtaining qualitative spatial distribution of *HC*, *C* and $CaCO_3$. Applying quantitative analysis such as Rietveld fitting for each pixel was not reliable since the relatively large size of some crystal particles (in particular cerussite), with respect to the beam size ended into highly oriented, quasi single crystal patterns. As an alternative, cumulated Debye-Scherrer rings were calculated using XRDUA, for an entire selected area of the crystalline map, more particularly over each layer of the paint stratification. With this approach, the signal is averaged over tens of grains, presenting disperse orientations, the resulting XRD pattern being more similar to a powder-like pattern. For each cumulated diffractogram, cerussite, hydrocerussite and calcite relative amounts were estimated on the basis of integrated intensities of a single, but strong and non-overlapped peak (*C* (021), *HC* (015)) (Fig. 2B, Fig. S.I.2). Values measured on standard mixtures were used to convert intensity ratios into weight ratios *HC*/*HC*+*C* (w%). The main asset of μXRD is the excellent spatial resolution, allowing discriminating paint layers with thickness of only several microns. However, several limitations related to the used geometry (some pigment grains having a size of the order of the beam size leading to preferential orientations; limited statistics due to the limited amount of material contributing to the diffracted signal) can skew the measured intensities, thus limiting the accuracy of the calculated composition. It is reasonable to envision a ±10 w% error bar for *HC*:*C* ratios.

Furthermore, the observation of the cumulated diffraction rings indicated a satisfactory statistic which allowed us to estimate the Scherrer broadening for *HC*, on the basis of the (015) and (107) peaks. In this case, the instrumental function was evaluated to 0.15° (2θ) on the basis of the $CaCO_3$ phase present in the sample, and FWHM for each peak was evaluated by fitting them independently using the Fullprof software. Considering a possible error of 2/100° during the FWHM measurement, the error on the crystal thickness is of about 120 nm.

RESULTS AND DISCUSSION

In order to provide explanations of the observed tendencies, the diffraction data obtained on historical samples was compared with results gathered on models samples. Those models have been obtained by reconstitution of the corrosion process and of post-synthesis treatments. Experiments will be detailed in a forthcoming publication, but we summarize here the main conclusions as a basis for the interpretation of results obtained on historical samples. First, these experiments highlighted the complexity of the corrosion process based on the combined action of acetic acid vapor, CO_2, O_2, H_2O: several intermediate phases (lead acetates) as well as plumbonacrite[25] $Pb_{10}(CO_3)_6O(OH)_6$ (*PN*) were detected in the first stage of corrosion, before their transformation in *HC* and *C*. As a rule of thumb, it appears that the lead white composition evolves during the corrosion process towards carbonate-rich phases, that is, from *PN* to *HC*, then *C*, but whereas *HC* and *C* form flakes that peel off easily, *PN* only occurs in the thin corrosion film that sticks to metal. Therefore, *PN* is only rarely observed in the final pigment. Besides, these reproductions showed that the amount of *C* increases with the corrosion time, as the *HC* → *C* transformation keeps going as long as CO_2 is present. So, if the CO_2 supply was too important, or continued after the consumption of the metallic lead, a pigment with *C* > *HC* was obtained. However, in a real stack process, the supply of CO_2 necessary to entirely convert *HC* into *C* was limited. Indeed, the *HC* → *C* reaction consumes five times as much CO_2 per Pb atom than the *PN* → *HC* reaction (see S.I.3): synthesizing an important amount of *C* is difficult. So, we expect an historical lead white to be mostly composed of *HC*.

In the same way, in the case of a brief synthesis, the ratio was displaced such as *HC* > *C* (up until *HC*:*C* = 100:0 w%). More detailed information on the reaction chain at stake in the stack process is presented in S.I.

Furthermore, the two main post-synthesis treatments frequently described in historical sources (heating in water, washing or grinding in vinegar)[26] were also reproduced on pure *HC* and *C* powders, to investigate their effects. It was thus observed that heating in water induced the transformation of *C* into *HC*, according to the following reaction:

$$3\ PbCO_3 + 2\ H_2O \rightarrow Pb_3(CO_3)_2(OH)_2 + H^+ + HCO_3^-$$

The newly formed *HC* crystallites were of important sizes, with dimensions up to 5 µm instead of < 1 µm without this post-process.

Conversely, the treatment in acidic environment of pure *HC* led to a formation of *C*, following a recrystallization process:

$$Pb_3(CO_3)_2(OH)_2 + 2\ CH_3COOH \rightarrow 2\ PbCO_3 + Pb^{2+} + 2\ CH_3COO^- + 2\ H_2O$$

As stated above, we will use those results (summarized in Fig. 3) to explain the composition and microstructure of the lead white pigment used by Old Masters in their paintings, accessible using SR-XRD.

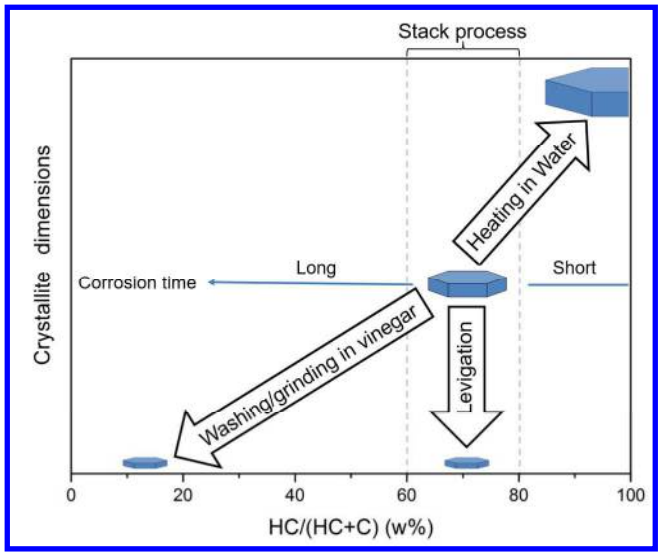

Figure 3 : Composition and microstructure of lead white as a function of synthesis conditions and post-synthesis processes

HR-SR-XRD

Composition Fig. 4 gives an overview of the compositions (*HC*/*HC*+*C* w% and $CaCO_3$/*HC*+*C* w%) measured on the entire corpus of raw micro-samples.

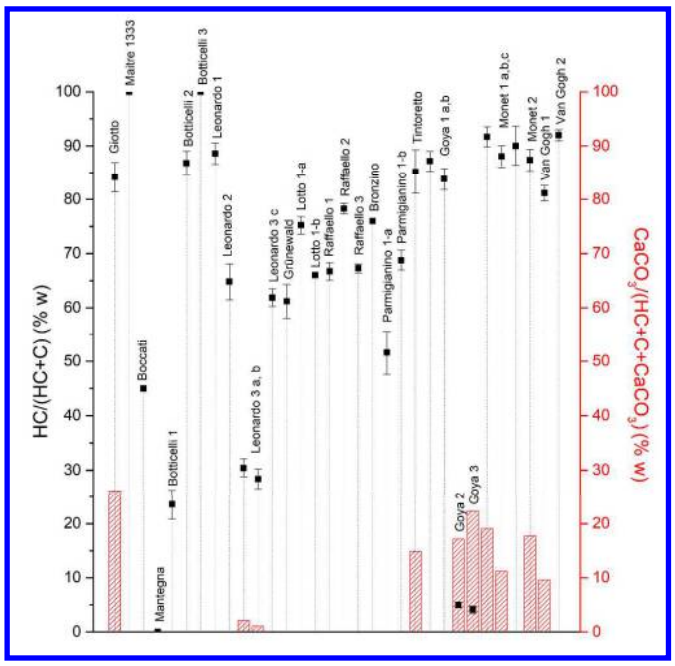

Figure 2 : Composition derived from Rietveld fitting of ID22 data. Hydrocerussite (left scale, black squares) and calcite (right scale, red bars) weight ratios. Samples are plotted in chronological order from left to right

Several observations can be made:

- From the 14th to the 19th c., most of the samples present a *HC*-rich chemical composition (*HC*:*C* ratio between 60:40 and 80:20 w%).
- Lead white pigments produced during the 19th c. are all very rich in HC (*HC*:*C* > 80:20 w%).
- Two samples are only composed of *HC* (Maitre 1333 and Botticelli 3).
- A small number of samples (8/34) present a *HC*:*C* < 50:50 w% ratio, meaning that they contain more *C* than *HC*.
- Calcite $CaCO_3$ is frequently present as an extender of lead white, sometimes in a very important amount (> 20 w%), and this more frequently from the late 19th c. (samples collected on paintings by Goya and Monet).

Relying on the laboratory reconstitution of the corrosion process and of the post-synthesis treatments (cf. Fig. 3), it is possible to propose explanations to those observations.

- The persistence in time of *HC*:*C* ratios comprise between 60:40 and 80:20 w% is noteworthy. As stated above, if a lead white synthesis is carried on until total lead depletion, a *C* > *HC* pigment would be expected. This persistence could then be explained by several reasons. First, as stated above, the supply of CO_2 necessary to entirely transform *HC* into *C* was limited in a stack. Another explanation is a systematic harvest of the pigment before complete consumption of lead. The reason for this could be a special interest of painters in *HC*-rich pigments: recent work suggest that the specific morphology of *HC* crystallites indeed communicates interesting optical properties to the pigment[27]. Finally, another possibility is an *C* → *HC* evolution of the pigment within paint layers over centuries, but this seems doubtful, as it would require a shift of *p*H towards basicity, which is unlikely in a polymerized fatty-acid organic binder. This leads us to the hypothesis that a pigment with a weight ratio *HC*:*C* comprise between 60:40 and 80:20 w% corresponds to the standard product obtained by the stack process.

- The very high *HC* amounts detected in samples from the 19th c. (*HC*:*C* > 80:20 w%) could be explained by two hypotheses. The first hypothesis is linked to the rate of the phases formation during this process. As mentioned before, *HC* is the first crystalline phase that forms abundantly during corrosion. As the demand for lead white was considerable at this time[28], production rates were increased and corrosion times were curbed at the maximum, which could lead to the formation of an even more *HC*-rich lead white. Secondly, all of the historical sources describing the synthesis of lead white during the 19th c. insist on the very thorough washing that was performed on the pigments in factories[29, 30]: such a post-synthesis treatment could also lead to an increase of the *HC* percentage.

- Ratios *HC*:*C* = 100:0 w% could result either from a very brief synthesis or from the heating of the pigment in water (the *HC* crystallites would then have a large size), as previously stated.

- Two main hypotheses can be considered for the *C*-rich samples. The first is that the *C* enrichment took place during the synthesis by the stack process. As described above, the transformation of all the *HC* created during the corrosion in *C* could for example result from a CO_2 supply sufficient for completing the carbonation, or a long corrosion time. The second is that a post-synthesis treatment in acidic environment (by washing or grinding) was used.

- Regarding the high amount of calcite sometimes mixed with the lead white (20 w% of $CaCO_3$ corresponds to 40% of the pigment volume), it is possible to deem that such pigments were of lower quality, as attested by numerous historical sources[31, 32]. The fact that most samples from the 19th c. contained calcite mixed with lead white is also in agreement with sources: the adjunction of this extender was frequent at those times, when the production of the lead white pigment could almost be qualified as industrial.

Microstructure When the amount of diffracting matter was sufficient (e.g. samples of size > 100 µm), HR-XRD diffractograms of high quality were obtained, enabling the modeling of *HC* and *C* crystallites, based on the anisotropic broadening. This modeling is unprecedented for lead white, as pigment crystallites are aggregated when the pigment is mixed with the binder, and thus unobservable by classic examination techniques used in conservation science such as scanning electron microscopy (SEM).

Crystallites shapes were in accordance with the expected model for the two phases (elongated rhombohedra for *C* and hexagonal platelets for *HC*). The obtained results can be divided into two temporal periods: 14-16th c. and 19th c., as visible on Fig. 5.

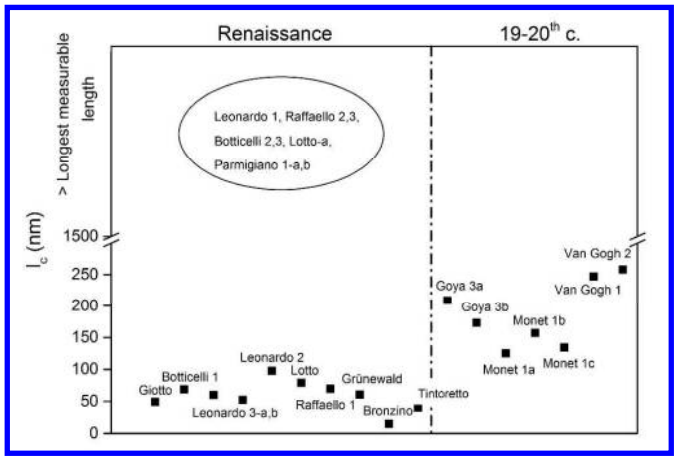

Figure 3 : Evolution of the mean HC crystallite sizes in time. For the 14-16th c. group, lead white exhibit either very small or large (superior to the longest measurable length) crystallites.

The first observation is that for lead whites used during the 14-16th c., samples split up into a bimodal distribution: a first group is composed of crystallites with sizes inferior to 150 nm, while another is constituted of particles with l_c > 1500 nm, that is to say superior to the longest measurable length.

Providing a definitive explanation of these tendencies is difficult, but several points for reflection can be made. Regarding the 14-16th c. period, the only synthesis method then used was the stack process. The presence of two groups of sizes could be ascribed to the use of a post-synthesis treatment. Indeed, heating the pigment in water could account for large-sized crystallites. Conversely, a treatment in vinegar inducing an acidic dissolution of *HC* crystallites could explain the presence of smaller particles. Finally, levigation of lead white was often performed, in order to select only the finest pigment particles[33]. This post-synthesis treatment could also result in a pigment composed of small crystallites.

Regarding the 19th c., it cannot be asserted that the stack process is the only used way to produce lead white. The increase in crystallites size could thus be the result of new synthesis routes developed at this time. However, the stack process was far from being abandoned and we can suppose that the better monitoring of the corrosion conditions (temperature control, gas flows…), or the thorough washing always performed in lead white factories, resulted in larger crystallites.

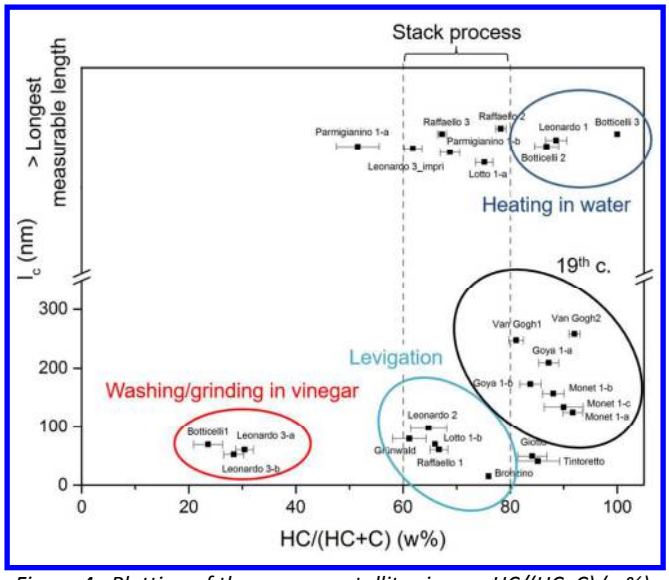

Figure 4 : Plotting of the mean crystallite sizes vs HC/(HC+C) (w%)

The plotting of *HC* crystallite mean sizes as a function of the *HC*:*C* ratio (Fig. 6) proves informative.

A first group of pigments rich in *C* and composed of small sizes particles appears. This supports the idea that this type of lead white could originate from a post-synthesis treatment in acidic conditions: the recrystallization of small *C* crystallites is accompanied by the dissolution of all the pre-existing crystallites: remaining *HC* platelets exhibit small dimensions. A second group of pigments used by artists of the 14-16th c. with small crystallites could be the result of a levigation process, that would permit to select only small crystallites without shifting the *HC*:*C* ratio. A third group composed of pigments containing HC crystallites of large dimensions and with *HC*:*C* > 80:20 w% could account for the heating of the pigment in water. Finally, lead whites used by painters of the 19th c. present comparable features (small crystallites with *HC*:*C* > 80:20), and could highlight the quasi-industrialization of the lead white synthesis at this time.

SR-µXRD

Qualitative µXRD crystalline maps were obtained on two samples, taken from the paintings of Beaumetz and Bellechose, as detailed in the introduction. Preliminary SEM observations of these two samples reveal comparable stratigraphies: on a thick Ca-based preparatory layer, successive lead white layers were painted: first a thin priming layer (marked #2 on Fig.

7A and 7B), then a pictorial layer (only one in the case of Beaumetz (#3 on Fig. 7A) and two for Bellechose (#3 and #4 on Fig. 7B). It is worth noting that in the case of Bellechose, a thick lead white-based transfer layer (not visible on the SEM image) is found below the calcite ground. This layer is not of origin and was not taken into account.

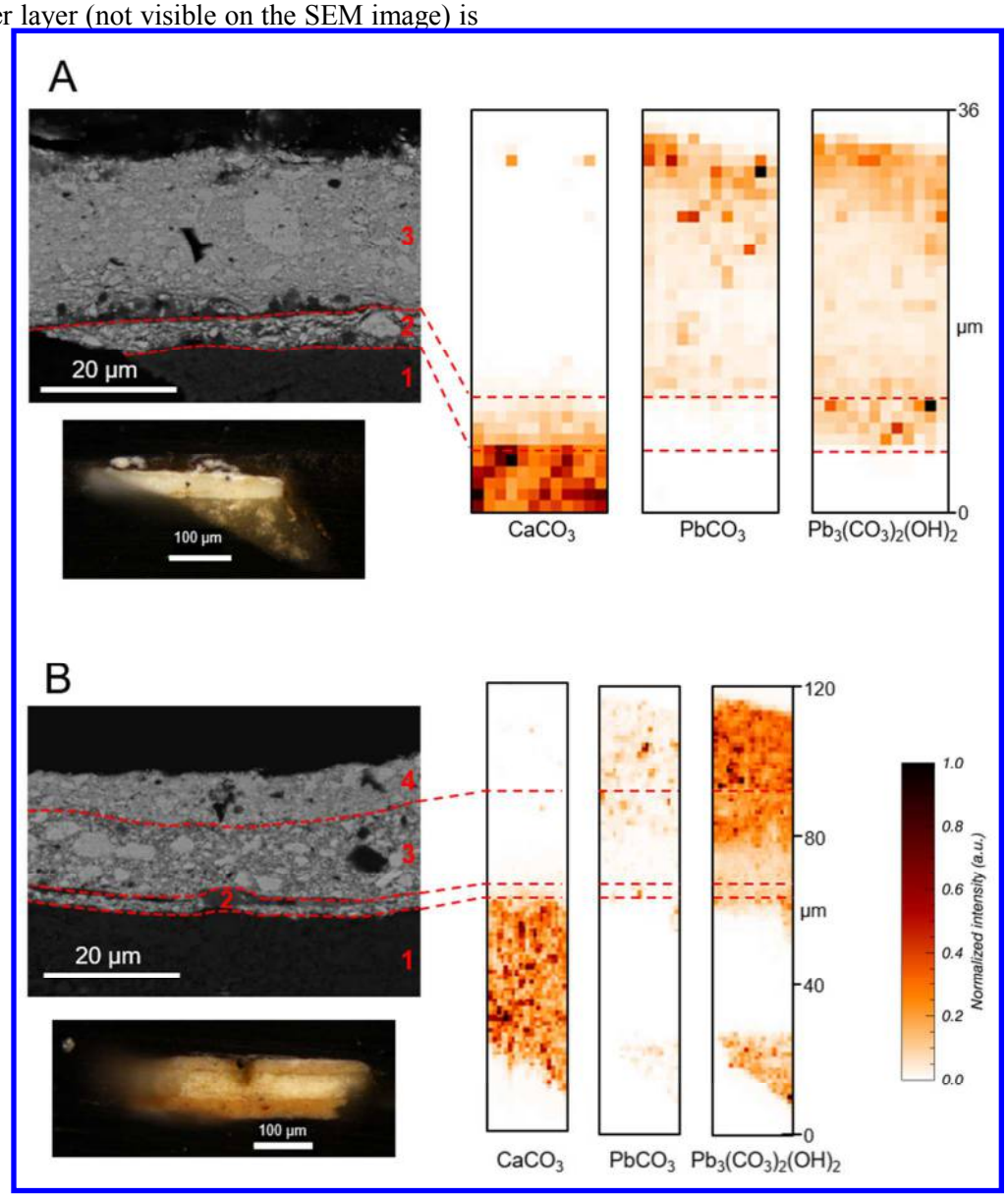

Figure 5 : Mapping of calcite $CaCO_3$, C $PbCO_3$ and HC ($Pb_3(CO_3)_2(OH)_2$), for the sample Beaumetz (A) and Bellechose (B). On the Beaumetz sample, above the calcite ground, the impression layer (delimited in red dots) only contains HC. On top the white layer contains a mix of HC and C. On the Bellechose sample, above the calcite ground several lead white layers containing HC and C are superimposed.

For the Beaumetz sample, the phase maps immediately render the stratification of the sample. The preparatory layer is composed of calcite $CaCO_3$. The priming layer is composed of 100% HC. The pictorial layer above is composed of a mix of the two carbonates with the estimated ratio *HC*:*C* = 75:25 (±10) w%.

For the Bellechose sample, the distinction of specific lead white recipes (i.e. specific *HC*:*C*) was not straightforward, due to the low chemical contrast between adjacent lead white layers #2, 3 and 4. In this case, layers were identified on the basis of the SEM images, showing characteristic pigment grain morphologies (see Fig. 7). Cumulated patterns were calculated over those regions. The following ratios were obtained for the lead white layers: for the priming (layer #2): *HC*:*C* = 80:20 (±10) w%, for layer #3: *HC*:*C* = 90:10 (±10) w%, for layer #4: *HC*:*C* = 80:20 (±10) w%. The limited precision of the ratio

estimations does not allow to discriminate potential pigment qualities between the layers.

Regarding lead white microstructure, for the lead whites used by Beaumetz, in the priming as well as in the pictorial layer, the broadening corresponds to *HC* platelets with a thickness of about 400 nm. For Bellechose, thickness of the *HC* platelets was estimated to 250 nm for the upper layer (#4) and 400 nm for the intermediate layer (#3). Taking into account the ±120 nm error corresponding to the FWHM estimation, the obtained thickness still corresponds to very important crystallite sizes.

Considering all the XRD information gathered on the two samples, we propose a possible identification on the *blanc de puille* used by Beaumetz as a lead white pigment composed of 100% *HC*. This composition is indeed particularly uncommon, and can either be linked to a post-synthesis treatment, or to specific synthesis conditions.

We showed that such a composition can be the result of the pigment heating in water. This first hypothesis is in agreement with the estimated crystallites sizes. We can propose that the name *blanc de puille* was given to a lead white sold in a poor state of cleanliness and that had to be washed for a long time by the painter himself, in order to get rid of impurities (dirt) it contained. This would account for the reduced price of *blanc de puille*: a low grade pigment requiring thorough washing to be usable in paintings.

Another hypothesis relies on the examination of another historic treatise. In this manuscript, the author affirms that *blanc de puille* was obtained using urine instead of vinegar during the pigment synthesis. This could also account for the high HC content observed. Indeed, the amount of CO_2 in such a synthesis would be considerably lesser than when vinegar is used. In the case of such a CO_2-deprived corrosion environment, the formation of hydrocerussite would conceivably be favored.

Finally, other white mineral compounds such as calcite $CaCO_3$ or *gesso* $CaSO_4.2H_2O$ have been ruled out, as the price of *blanc de puille* remains too high to designate those cheap materials.

It is worth noting that the only other sample we observed with a similar composition also stems from the same historic period (Maitre 1333 sample, see Fig. 4). The synthesis of *blanc de puille* could thus have been time-bound in Europe during the 14th c. before disappearing.

CONCLUSION

Using two SR-based XRD analytical configurations on historical micro-samples, it was possible to gain insight on the various grades of lead white pigments used by painters.

Variations of the hydrocerussite/cerussite ratios and of pigment crystallite sizes were connected to different synthesis conditions, or to post-synthesis treatments employed by paint manufacturers and artists of the past.

In addition, the use of μXRD allowed identifying a particular pigment used during the 14th C., reinforcing our knowledge of the use of paint materials during the Middle-Ages.

A previous study performed on reference samples has highlighted the effects of post-synthesis treatments on the pigment optical properties[34]. While many questions remain regarding their criteria when choosing between various grades of lead white, this work allowed taking a step forward in the understanding of the pictorial practices of the Old Masters.

Regarding methodology, an important consideration is the high complementarity of the various SR-XRD configurations that were implemented. While the excellent data quality of the HR-XRD permits a very precise estimation of the studied material composition and microstructure, only the spatial resolution of the μXRD allows to distinguish between paint layers at the micro-scale.

The main limitation of SR-XRD as used here is that it is applied on samples of micrometric dimensions. The issue of reproducibility, despite having been successfully tested on some samples collected on the same painting[14], remains open. Regarding this issue, recent instrumental developments, especially crystalline phase mapping at the macro scale are

promising[35]. The combination of those new laboratory-based instruments with methodologies described in this work could provide even more detailed information on the Old Masters pictorial practices.

ASSOCIATED CONTENT

Supporting information available

Protocol for thin-section preparation at ID21; Calibrating curve based on standard *HC*/*C* mixtures for the quantification of phases at ID21; Information regarding the chemical reactions at stake during the synthesis and post-synthesis of lead white ; List of historical micro-samples analyzed in this study indicating the museum in which each painting is conserved.

AUTHOR INFORMATION

Corresponding Author

* Victor Gonzalez, gonzalvic@gmail.com

Author Contributions

XRD data was collected during 3 beamtime sessions at the ESRF by V.G., G.W., T.C., M.C., W.D.N and M.M. Data treatment was performed by V.G., G.W. and W.D.N. The ensemble of results was discussed between all authors. The paper was written by V.G., M.C. and G.W. All authors have given approval to the final version of the manuscript.

Notes

The authors declare no competing financial interest.

ACKNOWLEDGMENT

We acknowledge the ESRF for providing beamtime. We are indebted to Andrew N. Fitch for support at the ID22 beamline, and Tiphaine Fabris at the ID21 beamline. This work was funded by the French *Ministère de la Culture* and by the ED388 of *Université Pierre & Marie Curie* (UPMC), Paris.

REFERENCES

1. Gettens, R. J.; Kühn, H.; Chase, W. T. *Stud. Conserv.* **1967,** *12*, 125-139.
2. Chevrier, C.; Giester, G.; Heger, G.; Jarosch, D.; Wildner, M.; Zemann, J. *Zeitschrift für Kristallographie* **1992,** *199*, 67-74.
3. Martinetto, P.; Anne, M.; Dooryhee, E.; Walter, P.; Tsoucaris, G. *Acta Cryst. C* **2002,** *58*, 82-84.
4. Franke, W.; Lenk, K. *J. of Cryst. Growth* **1981,** *51*, 309-313.
5. Sánchez-Navas, A.; López-Cruz, O.; Velilla, N.; Vidal, I. *J. of Cryst. Growth* **2013,** *376*, 1-10.
6. Shahwan, T.; Zunbul, B.; Akar, D. *Geochem. J.* **2005,** *39*, 317-326.
7. Welcomme, E.; Walter, P.; Van Elsande, E.; Tsoucaris, G. *App. Phys. A* **2006,** *83*, 551-556.
8. Harley, R. D. In *Artists' Pigments c. 1600-1835, A study in English documentary sources, 2nd revised ed.*; Butterworth Scientific: London, 1982.
9. Tétreault, J.; Sirois, J.; Stamatopoulou, E. *Stud. Conserv.* **1998,** *43*, 17-32.
10. Merrifield, M. P. In *Original Treatises on the Arts of Painting*.; Dover Publications, Inc.: New-York, 1849.
11. Stols-Witlox, M. In *Studying Old Master Paintings - Technology and Practice*; Archetype Publications: London, 2011; pp. 284-290.
12. Pulsifer, W. H. *Notes for a history of lead and an inquiry into the development of the manufacture of white lead and lead oxides*; D. van Nostrand: New-York, 1888.
13. Kubersky-Piredda, S., In *Trade in artist's materials*; Archetype Publications: London, 2010; pp 223-243.
14. Gonzalez, V.; Calligaro, T.; Wallez, G.; Eveno, M.; Toussaint, K.; Menu, M., *Microchem. J.* **2016,** *125*, 43-49.
15. Nash, S. In *Trade in artist's materials*; Archetype Publications: London, 2010; pp 97-142.
16. Corbeil, M. C.; Sirois, P. J. *Stud. Cons.* **2007,** *52*, 281-288.
17. Stols-Witlox, M.; Megens, L.; Carlyle, L. In *The Artist's Process : Proceedings of the fourth symposium of the Art Technological Source Research Working Group*; Archetype Publications: London, 2012; pp. 112-120.
18. Pouyet, E.; Lluveras-Tenorio, A.; Nevin, A.; Saviello, D.; Sette, F.; Cotte, M. *Anal. Chim. Acta* **2014,** *822*, 51-59.
19. Pouyet, E.; Fayard, B.; Salome, M.; Taniguchi, Y.; Sette, F.; Cotte, M. *Heritage Sci.* **2015,** *3*, 1-31.
20. Hodeau, J. L.; Bordet, P.; Anne, M.; Prat, A.; Fitch, A. N.; Dooryhee, E.; Vaughan, G.; Freund, A. K., *Proc. of SPIE*, **1998**, 3448, 353-361.
21. Rietveld, H. M. *J. Appl. Crystallogr.* **1969,** *2*, 65-71.

22. Rodriguez-Carvajal, J. *Physica B.* **1993,** *192*, 55-69.
23. Cotte, M.; Pouyet, E.; Salome, M.; Rivard, C.; De Nolf, W.; Castillo-Michel, H.; Fabris, T.; Monico, L.; Janssens, K.; Wang, T.; Sciau, P.; Verger, L.; Cormier, L.; Dargaud, O.; Brun, E.; Bugnazet, D.; Fayard, B.; Hesse, B.; Pradas del Real, A. E.; Veronesi, G.; Langlois, J.; Balcar, N.; Vandenberghe, Y.; Sole, V. A.; Kieffer, J.; Barrett, R.; Cohen, C.; Cornu, C.; Baker, R.; Gagliardini, E.; Papillon, E.; Susini, J., *J. Anal. At. Spectrom.* **2017,** *32*, 477-493.
24. Ashiotis, G.; Deschildre, A.; Nawaz, Z.; Wright, J. P.; Karkoulis, D.; Picca, F. E.; Kieffer, J., *J. Appl. Crystallogr.* **2015,** *48*, 510-519.
25. De Nolf, W.; Vanmeert, F.; Janssens, K., *J. Appl. Crystallogr.* **2014,** *47*, 1107-1117.
26. Cotte, M.; Fabris, T.; Agostini, G.; Motta Meira, D.; De Viguerie, L.; Sole, V. A., *Anal. Chem.* **2016,** *88*, 6154-6160.
27. Gonzalez, V. Caractérisation microstructurale et luminescence des carbonates de plomb : apport à la discrimination des pigments blancs de plomb des oeuvres peintes. Ph.D. Thesis, Sorbonne University, UPMC Univ, Paris, October 2016.
28. Holley, C. D., *The lead and zinc pigments*. 1st ed.; John Wiley & Sons: New-York, 1909.
29. Bradshaw, W. R. *The Decorator and Furnisher* **1890,** *16*, 23-26.
30. Goodell, O. D., *White lead and its substitutes*; D. Oliver: Detroit, 1892.
31. Bruquetas, R. In. *The Artist's Process : Proceedings of the fourth symposium of the Art Technological Source Research Working* Group; Archetype Publications: London, 2012; pp. 138-146.
32. Dossie, R. *The handmaid to the arts*. J. Nourse: Londres, 1758.
33. De Behault, S. *Proc. of CREATE Conf.* **2010**, 86-90.
34. Gonzalez, V.; Gourier, D.; Calligaro, T.; Toussaint, K.; Wallez, G.; Menu, M., *Anal. Chem.* **2017,** *89*, 2909-2918.
35. De Nolf, W.; Dik, J.; Vandersnickt, G.; Wallert, A.; Janssens, K., *J. Anal. At. Spectrom.* **2011,** *26*, 910-916.

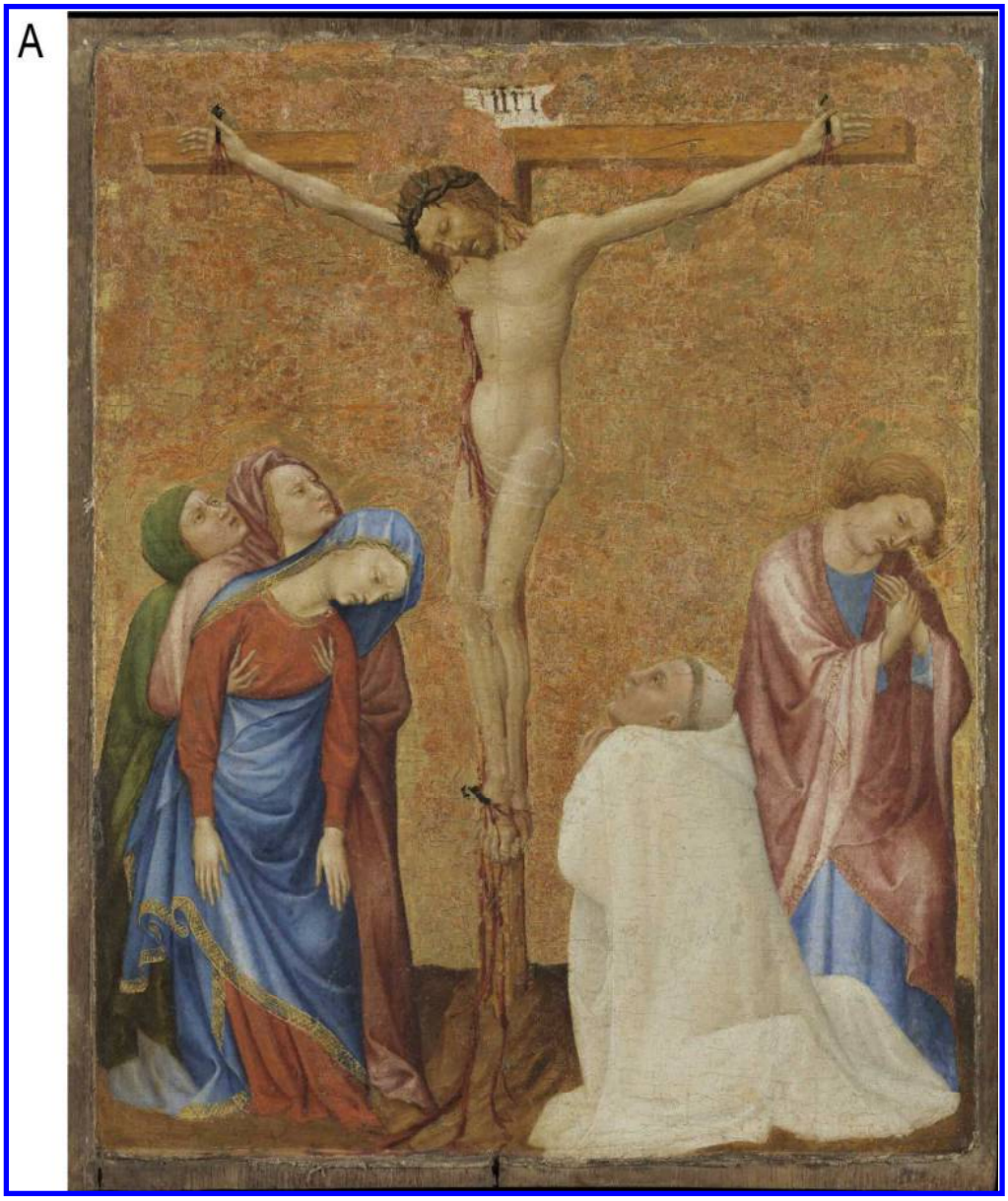

Calvaire avec un moine chartreux (c. 1395) by Jean de Beaumetz (Musée du Louvre, © C2RMF, 61 x 48.5 cm)

446x533mm (96 x 96 DPI)

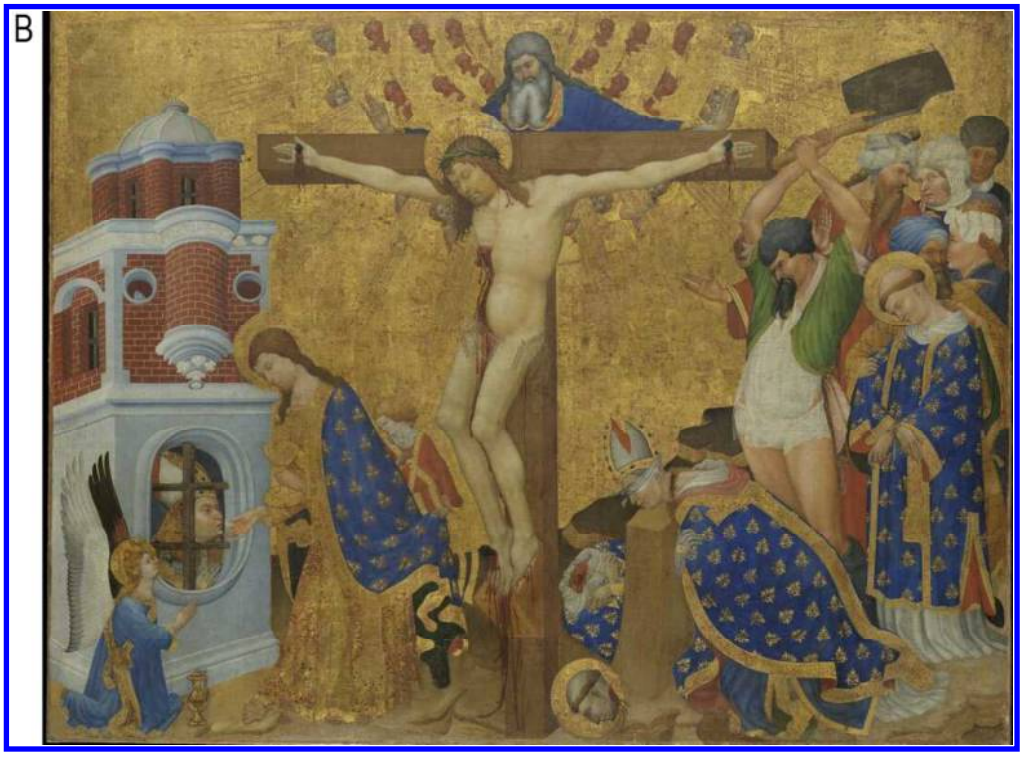

Retable de Saint Denis (1416) by Henri Bellechose (Musée du Louvre, © C2RMF, 162 x 211 cm)

284x208mm (96 x 96 DPI)

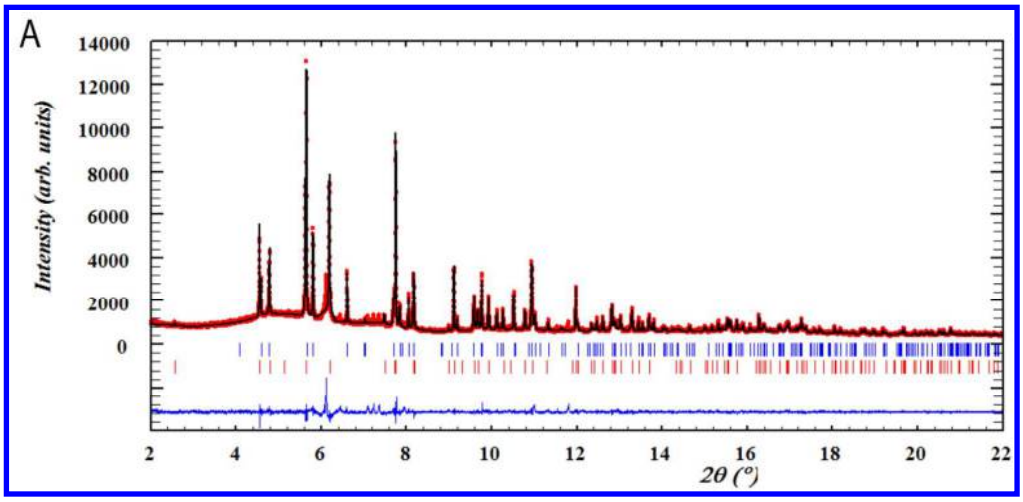

Rietveld plot for diffractogram recorded by HR-XRD at ID22 (sample Rafaello 1) : experimental (red circles), calculated (black line), difference (blue line), Bragg positions (bars)

280x134mm (143 x 143 DPI)

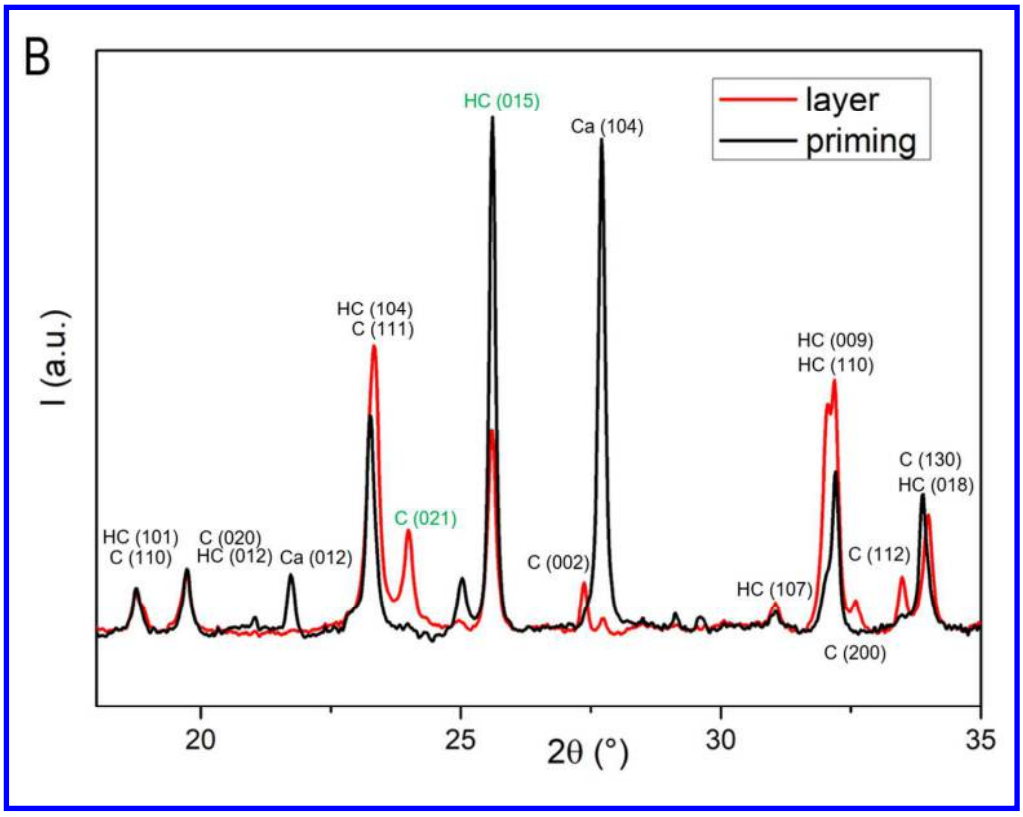

Cumulated and azimuthally integrated diffractogram recorded by μXRD at ID21 on layer 3 of sample Beaumetz (cf. Fig 7). Peaks used for quantification ($C_{(021)}$ and $HC_{(015)}$) are indicated in green

328x260mm (95 x 95 DPI)

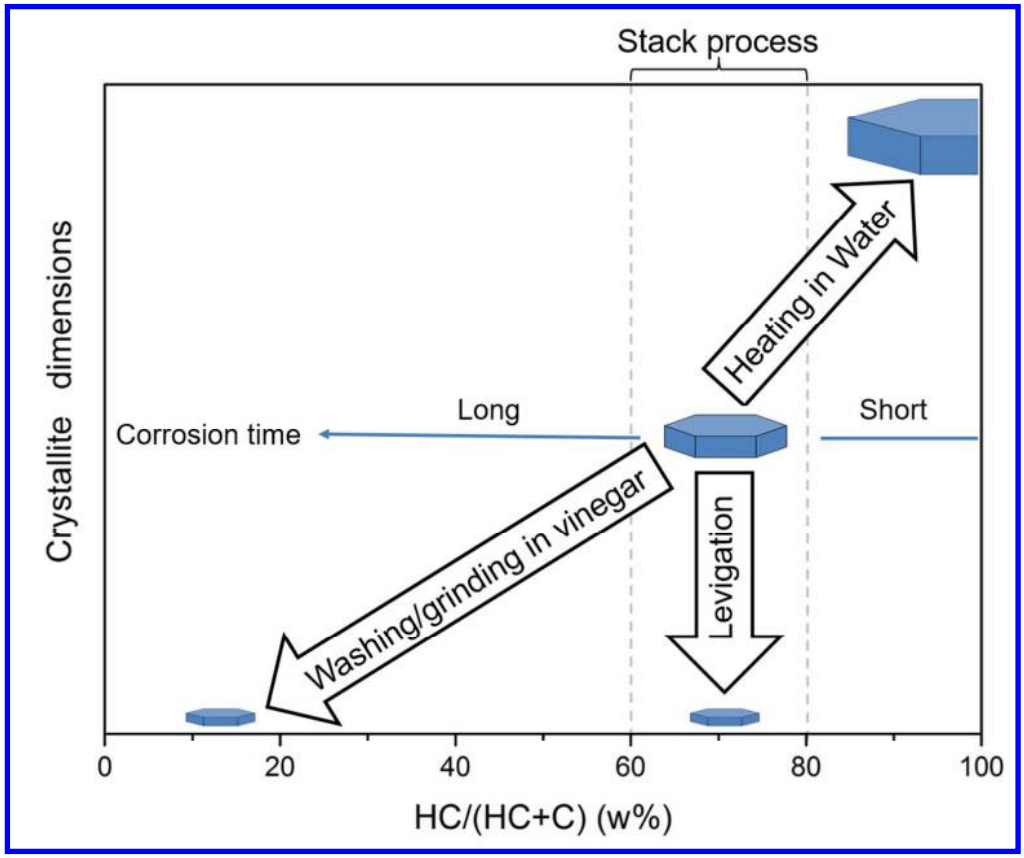

Composition and microstructure of lead white as a function of synthesis conditions and post-synthesis processes

206x172mm (144 x 144 DPI)

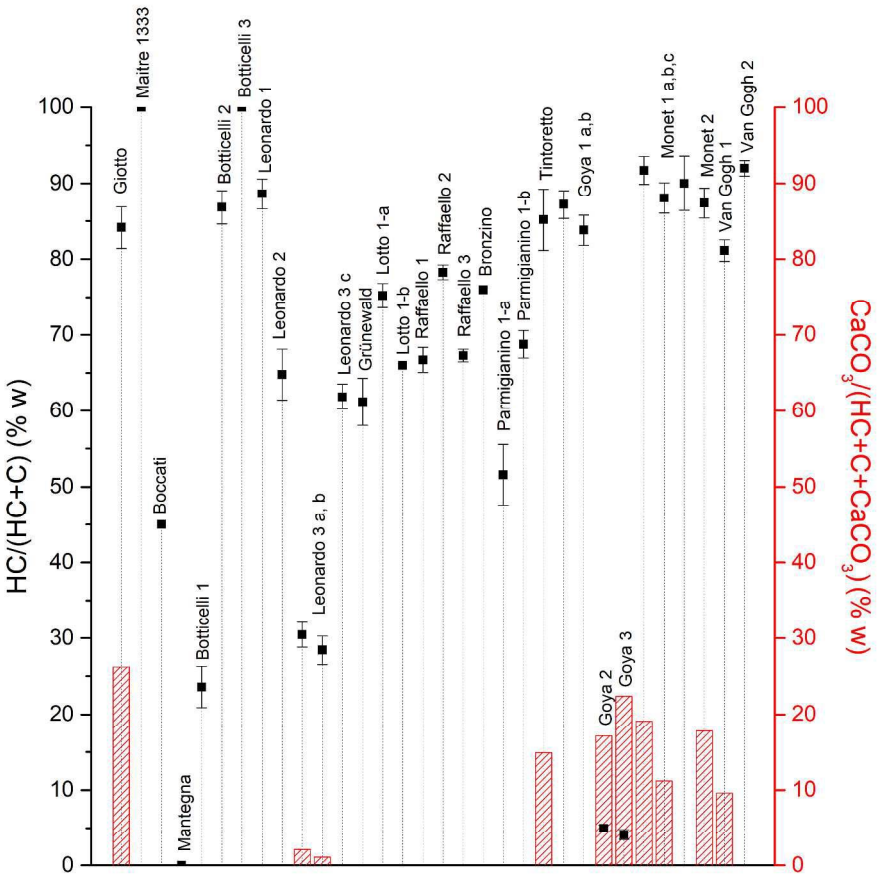

Composition derived from Rietveld fitting of ID22 data. Hydrocerussite (left scale, black squares) and calcite (right scale, red bars) weight ratios. Samples are plotted in chronological order from left to right

289x305mm (299 x 299 DPI)

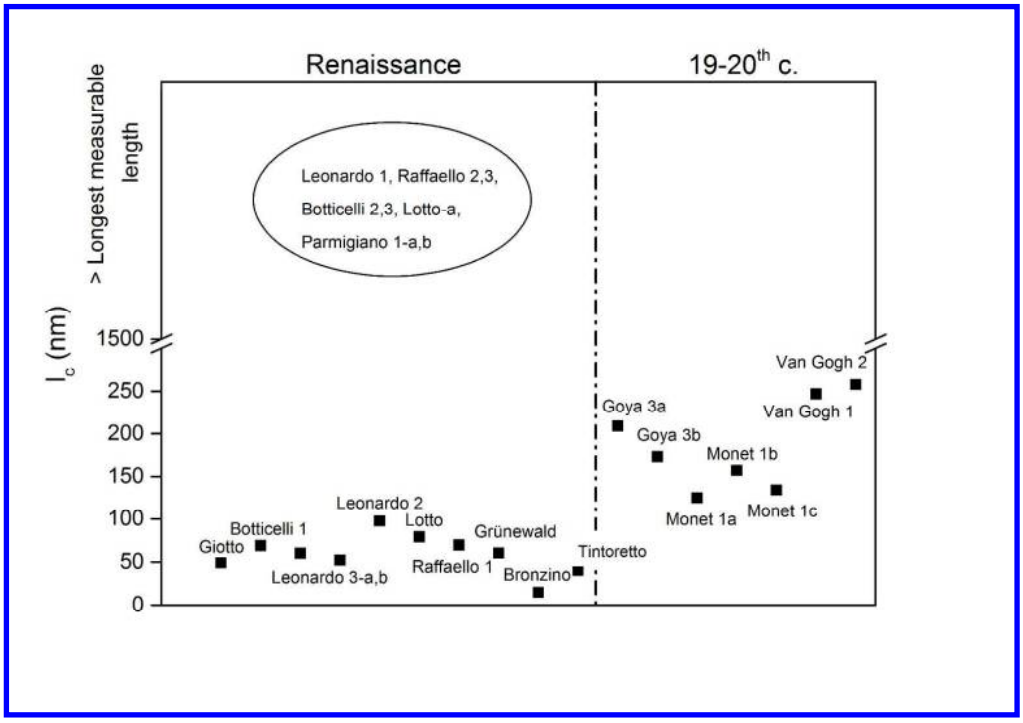

Evolution of the mean *HC* crystallite sizes in time. For the 14-16th c. group, lead white exhibit either very small or large (superior to the longest measurable length) crystallites.

288x201mm (300 x 300 DPI)

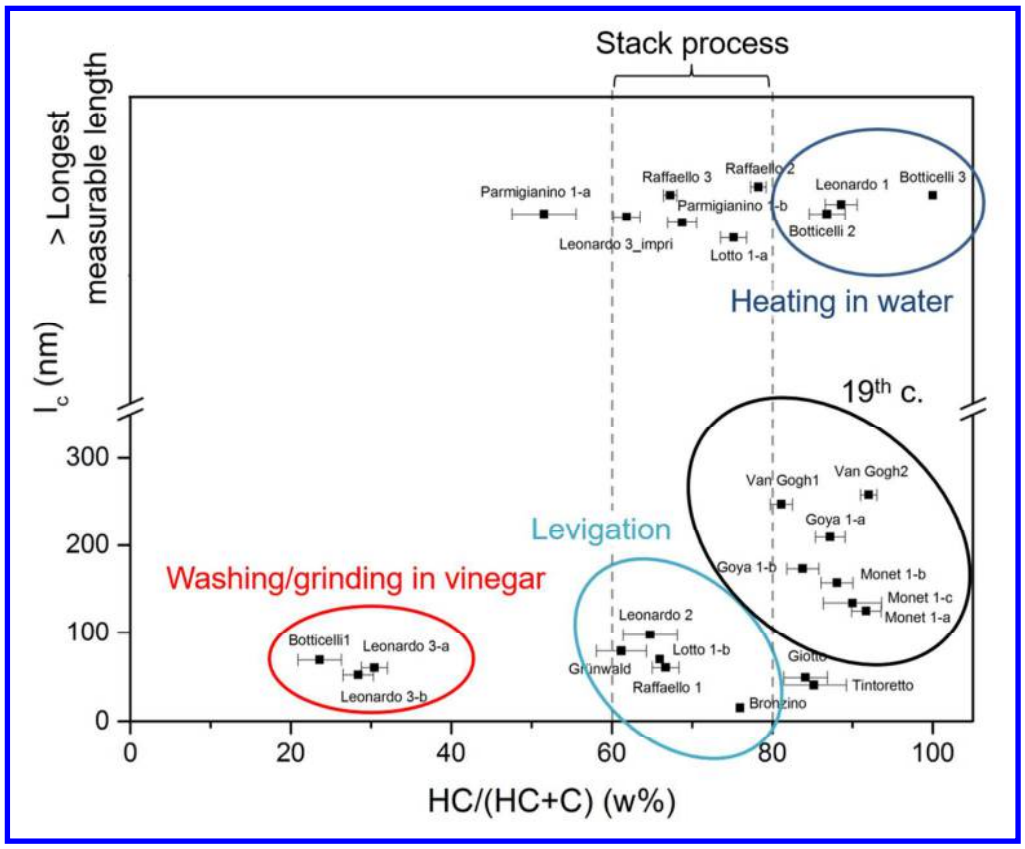

Plotting of the mean crystallite sizes vs *HC*/(*HC*+*C*) (w%)

214x177mm (144 x 144 DPI)

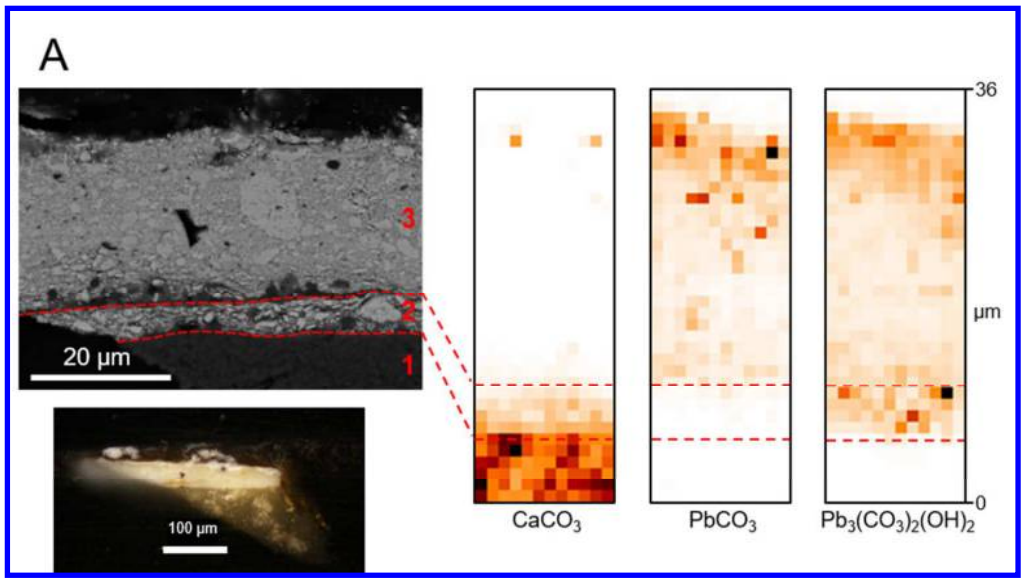

Mapping of calcite $CaCO_3$, *C* $PbCO_3$ and *HC* ($Pb_3(CO_3)_2(OH)_2$), for the sample Beaumetz (A) and Bellechose (B). On the Beaumetz sample, above the calcite ground, the impression layer (delimited in red dots) only contains *HC*. On top the white layer contains a mix of *HC* and *C*. On the Bellechose sample, above the calcite ground several lead white layers containing *HC* and *C* are superimposed.

151x84mm (144 x 144 DPI)

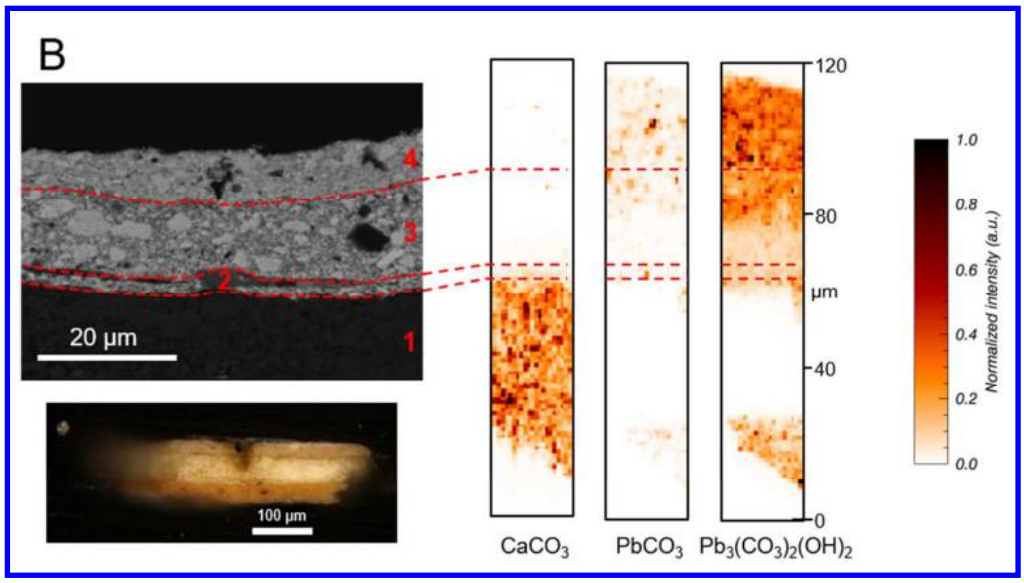

Mapping of calcite $CaCO_3$, *C* $PbCO_3$ and *HC* ($Pb_3(CO_3)_2(OH)_2$), for the sample Beaumetz (A) and Bellechose (B). On the Beaumetz sample, above the calcite ground, the impression layer (delimited in red dots) only contains *HC*. On top the white layer contains a mix of *HC* and *C*. On the Bellechose sample, above the calcite ground several lead white layers containing *HC* and *C* are superimposed.

228x127mm (96 x 96 DPI)

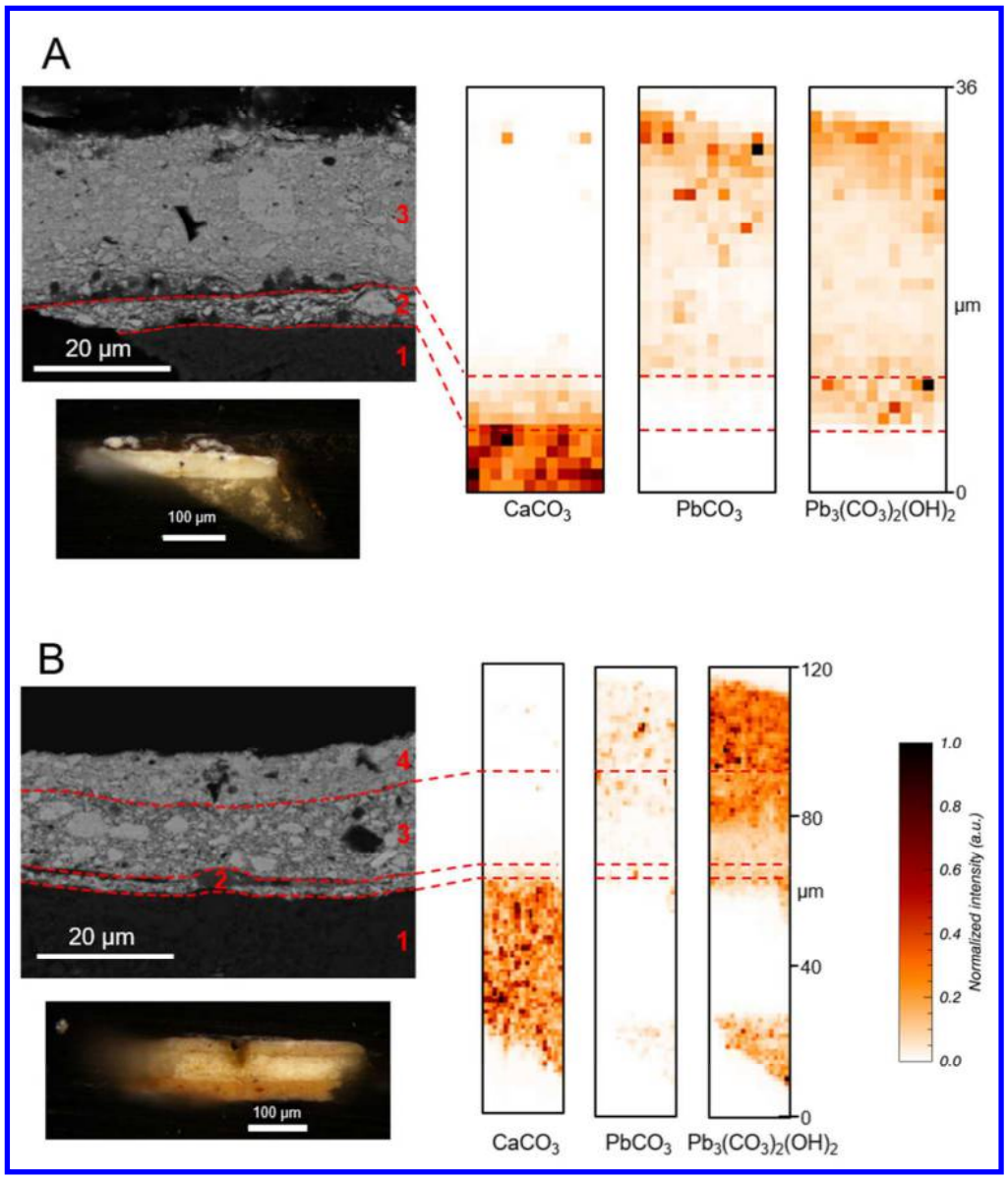

Mapping of calcite $CaCO_3$, *C* $PbCO_3$ and *HC* ($Pb_3(CO_3)_2(OH)_2$), for the sample Beaumetz (A) and Bellechose (B). On the Beaumetz sample, above the calcite ground, the impression layer (delimited in red dots) only contains *HC*. On top the white layer contains a mix of *HC* and *C*. On the Bellechose sample, above the calcite ground several lead white layers containing *HC* and *C* are superimposed.

228x268mm (96 x 96 DPI)

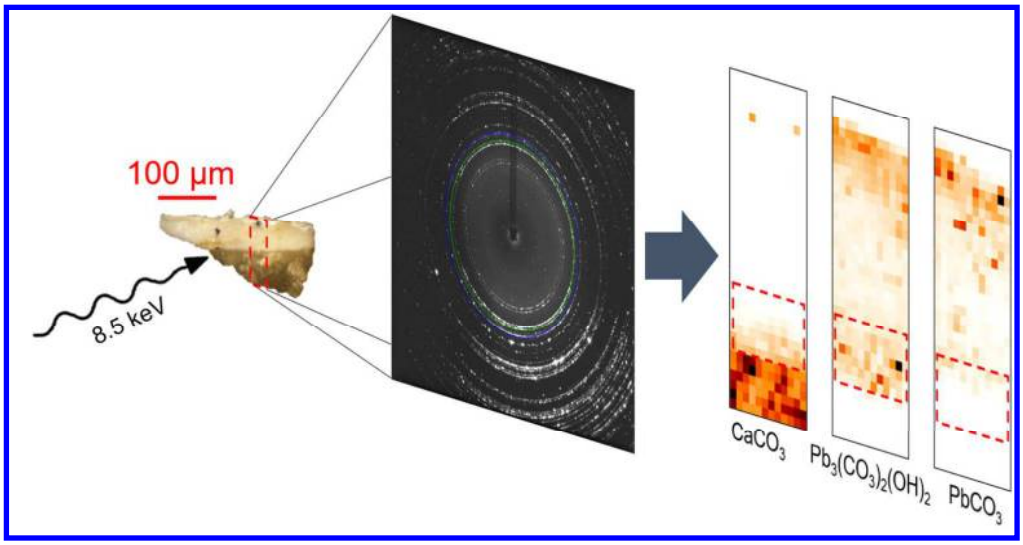

TOC

241x125mm (149 x 149 DPI)